Mirrored changes in Antarctic ozone and stratospheric temperature in the late 20th versus early 21st centuries

Citation: Solomon, Susan, Diane Ivy, Mukund Gupta, Justin Bandoro, Benjamin Santer, Qiang Fu, Pu Lin, Rolando R. Garcia, Doug Kinnison, and Michael Mills. "Mirrored Changes in Antarctic Ozone and Stratospheric Temperature in the Late 20th Versus Early 21st Centuries." Journal of Geophysical Research: Atmospheres 122, no. 16 (August 23, 2017): 8940–8950. © 2017 American Geophysical Union.

As Published: https://doi.org/10.1002/2017JD026719

Publisher: American Geophysical Union (AGU)

Persistent URL: http://hdl.handle.net/1721.1/121130

Version: Final published version: final published article, as it appeared in a journal, conference proceedings, or other formally published context

AGU PUBLICATIONS

JGR

Journal of Geophysical Research: Atmospheres

RESEARCH ARTICLE
10.1002/2017JD026719

Key Points:
- Pre- and post-2000 observed Antarctic ozone and temperature changes largely follow a "mirrored" pattern of sign reversals near 70–150 hPa
- An interactive chemistry-climate model produces broadly similar mirroring only when forced by ozone depleting substances
- The results support the recent finding that the healing of the Antarctic ozone hole is underway

Supporting Information:
- Supporting Information S1

Correspondence to:
S. Solomon,
solos@mit.edu

Citation:
Solomon, S., D. Ivy, M. Gupta, J. Bandoro, B. Santer, Q. Fu, P. Lin, R. R. Garcia, D. Kinnison, and M. Mills (2017), Mirrored changes in Antarctic ozone and stratospheric temperature in the late 20th versus early 21st centuries, *J. Geophys. Res. Atmos.*, *122*, 8940–8950, doi:10.1002/2017JD026719.

Received 25 FEB 2017
Accepted 7 AUG 2017
Accepted article online 11 AUG 2017
Published online 23 AUG 2017

Mirrored changes in Antarctic ozone and stratospheric temperature in the late 20th versus early 21st centuries

Susan Solomon[1], Diane Ivy[1], Mukund Gupta[1], Justin Bandoro[1], Benjamin Santer[2], Qiang Fu[3], Pu Lin[4], Rolando R. Garcia[5], Doug Kinnison[5], and Michael Mills[5]

[1]Department of Earth, Atmospheric, and Planetary Sciences, Massachusetts Institute of Technology, Cambridge, Massachusetts, USA, [2]Program for Climate Model Diagnosis and Intercomparison, Lawrence Livermore National Laboratory, Livermore, California, USA, [3]Department of Atmospheric Sciences, University of Washington, Seattle, Washington, USA, [4]NOAA Geophysical Fluid Dynamics Laboratory, Princeton Forrestal Campus, Princeton, New Jersey, USA, [5]Atmospheric Chemistry Observations and Modeling Laboratory, National Center for Atmospheric Research, Boulder, Colorado, USA

Abstract Observed and modeled patterns of lower stratospheric seasonal trends in Antarctic ozone and temperature in the late 20th (1979–2000) and the early 21st (2000–2014) centuries are compared. Patterns of pre-2000 observed Antarctic ozone decreases and stratospheric cooling as a function of month and pressure are followed by opposite-signed (i.e., "mirrored") patterns of ozone increases and warming post-2000. An interactive chemistry-climate model forced by changes in anthropogenic ozone depleting substances produces broadly similar mirrored features. Statistical analysis of unforced model simulations (from long-term model control simulations of a few centuries up to 1000 years) suggests that internal and solar natural variability alone is unable to account for the pattern of observed ozone trend mirroring, implying that forcing is the dominant driver of this behavior. Radiative calculations indicate that ozone increases have contributed to Antarctic warming of the lower stratosphere over 2000–2014, but dynamical changes that are likely due to internal variability over this relatively short period also appear to be important. Overall, the results support the recent finding that the healing of the Antarctic ozone hole is underway and that coupling between dynamics, chemistry, and radiation is important for a full understanding of the causes of observed stratospheric temperature and ozone changes.

1. Introduction

The springtime decrease in ozone abundances over Antarctica occurred rapidly between the late 1970s and early 1990s and was driven by anthropogenic emissions of chlorofluorocarbons and bromocarbons [e.g., *Solomon*, 1999, and references therein]. Due to the global phase out of these industrial chemicals under the Montreal Protocol, the Antarctic ozone "hole" stabilized around the late 1990s, and it has been shown using models and observations that the onset of slow healing began around 2000 [*Solomon et al.*, 2016]. Ozone loss was accompanied by marked stratospheric cooling. Here we present observations and model calculations showing that the seasonal and vertical patterns of trends in both Antarctic ozone and temperature in the lower stratosphere have systematically reversed when the decades before and after 2000 are compared. In this paper, we compare seasonal trends during what will be referred to as the "depletion era" of the late 20th century (1979–2000, 22 years inclusive; hereafter referred to as L1) and the "healing era" of the 21st century (2000–2014, 15 years inclusive; hereafter referred to as L2). To estimate the likelihood that the ozone trends and their reversal could have occurred by chance, we also analyze modeled ozone trends from multicentury control runs.

Ozone provides the principal source of heat to the stratosphere. The extensive depletion of Antarctic ozone in the late 20th century led to a strong radiatively driven stratospheric cooling [*Shine*, 1986; *Ramaswamy et al.*, 1996; *Forster and Shine*, 1997; *Randel and Wu*, 1999]. Studies suggest that the Antarctic ozone hole has affected stratospheric dynamics, although greenhouse gas increases during the same period also have contributed to the dynamical changes [e.g., *Thompson and Solomon*, 2002; *Manzini et al.*, 2003; *Cai*, 2006; *Son et al.*, 2009; *Butchart et al.*, 2010; *McLandress et al.*, 2010; *Lin and Fu*, 2013; *Oberländer-Hayn et al.*, 2015]. During the last several decades of the 20th century, Antarctic lower stratospheric temperatures were influenced not only by cooling linked to ozone losses but also by dynamical warming via increased

Table 1. Model Simulations

Model	Abbreviated Description	Period Considered	Forcings	Name of Simulation
FR-WACCM	Free-running coupled chemistry-climate	1979–2014	CCMI historical forcings	ODS + GHG FR-WACCM
FR-WACCM	Free-running coupled chemistry-climate	1979–2014	Only ODS, GHG fixed at 1960 value	ODS only
FR-WACCM	Free-running coupled chemistry-climate	1979–2014	Only GHG, ODS fixed at 1960 value	GHG only
FR-WACCM	Free-running preindustrial control run	1650–1850	None	CTL
FR-WACCM	Free-running preindustrial control run	850–1850	Solar	NAT
SD-WACCM	Specified dynamics, nudged to MERRA	1979–2014	CCMI historical forcings	ODS + GHG SD-WACCM
SD-WACCM	Specified dynamics, nudged to MERRA	2000–2014	Chemistry, dynamics, and volcanoes	Chem-dyn-vol
SD-WACCM	Specified dynamics, kept fixed at 1999 values throughout	2000–2014	ODS only	Chem-only

downwelling [*Lin et al*., 2009; *Calvo et al*., 2012; *Ivy et al*., 2016]. The Antarctic ozone loss is extremely sensitive to temperature, and a difference of a degree or so in the spring season substantially influences chemical loss rates [*Rex et al*., 2004; *Sinnhuber et al*., 2011; *Solomon et al*., 2015]. Antarctic ozone depletion thus involves coupling and feedbacks among chemistry, radiation, and dynamics and is a strongly seasonal phenomenon that extends mainly from late austral winter through summer. We study these interactions here using several different model configurations (see Table 1). First, we compare key features of the seasonal patterns in the depletion and healing eras using (1) station-based observations; (2) free-running dynamical-chemical model simulations; and (3) chemical simulations nudged to observed temperatures and winds. We then analyze solar and internal variability in long model control runs and compare the results to the forced trends obtained in modern simulations (late 20th and early 21st centuries). Finally, we examine the radiative components of temperature change arising from modeled ozone changes in the modern period. The next section describes the data sets and simulations used.

2. Data Sets and Model Simulations

Balloonsonde ozone measurements for the South Pole and Syowa stations are available at the National Oceanic and Atmospheric Administration (NOAA; esrl.noaa.gov/gmd/dv/spo_oz) and World Ozone and Ultraviolet Radiation Data Centre (WOUDC; woudc.org) archives, respectively. Antarctic total ozone monitoring began around the late 1950s. Vertical profiling from balloon records is more limited; profile data before the depletion era began are extremely limited. The long balloon records at the two stations were reviewed and compared in *Solomon et al*. [2005]. Data records from both stations are available beginning in the mid-1960s, but sampling is sporadic prior to the mid-1980s (see Table 1 in *Solomon et al*. [2005]). Data are not available at South Pole from 1976 to 1986, and there are also breaks in the data at Syowa. To optimize the temporal coverage in the predepletion period, we used all ozone observations at each station from 1966 to 1975 to define the reference period for ozone trend estimates.

The model framework used in this paper is the Community Earth System Model version 1 (CESM1), with the Whole Atmosphere Community Climate Model version 4, as the atmospheric component (WACCM4) [see *Marsh et al*., 2013]. WACCM4 is a detailed climate-chemistry model that extends from the Earth's surface to the lower thermosphere. We employ several complementary components of the WACCM modeling package, all with the same resolution in the lower stratosphere: (i) free-running simulations that include an interactive ocean component along with coupled chemistry and dynamics (referred to here as FR-WACCM) [see *Marsh et al*., 2013], (ii) specified-dynamic simulations that are constrained by observed temperatures and winds (SD-WACCM) [see *Solomon et al*., 2015, 2016, and references therein], and (iii) the radiative submodel of WACCM, the Parallel Offline Radiative Transfer (PORT) model [*Conley et al*., 2013]. SD-WACCM is constrained with reanalysis temperature and wind fields that are taken from two sources: the Modern Era Retrospective Analysis for Research and Applications (MERRA) [*Rienecker et al*., 2011], available for 1979 through 2014, and the Goddard Earth Observing System operational data for 2015. The procedure used to constrain SD-WACCM is described by *Marsh* [2011] and *Kunz et al*. [2011]. MERRA data are also used to provide estimates of observed temperature trends.

The chemical scheme and SD-WACCM test runs used here are the same as those discussed in *Solomon et al*. [2015, 2016] and have been shown to reliably represent the observed seasonal and interannual changes in Antarctic ozone. From 1979 to 2000, the SD-WACCM and FR-WACCM simulations are consistent with the

Chemistry-Climate Model Intercomparison (CCMI) hindcast forcings and employ the prescribed aerosol inputs from the CCMI aerosol evolution [*Arfeuille et al*., 2013]. A run of SD-WACCM using CCMI chemistry and aerosols was performed to provide a predepletion baseline (hereafter CCMI baseline) [see *Morgenstern et al*., 2017]. Since MERRA data are only available post-1979, this run repeatedly imposed the MERRA meteorological fields for the years 1979–1981 throughout the 30 year period from 1952 to 1978. Ozone depleting substances and greenhouse gases were allowed to change over time according to the REFC1 scenario [see *Morgenstern et al*., 2017]. After year 2000, SD-WACCM was used to perform two numerical experiments: a chemistry-dynamic volcano (hereafter referred to as "chem-dyn-vol") simulation with a detailed representation of volcanic activity post-2000 [see *Mills et al*., 2016; *Solomon et al*., 2016] and a chemistry-only (hereafter referred to as "chem-only") simulation in which 1999 dynamics and temperatures were imposed for all years after that date, so that only chemical changes contribute to the post-2000 ozone evolution in this case.

All least-squares linear trends were calculated from time series of monthly mean data. The year 2002 displayed very unusual meteorological characteristics in Antarctica and was not included in the trend analyses [*Scaife et al*., 2005]. Results are presented for the period up to 2014, avoiding the anomalous year 2015, when the Calbuco volcanic eruption enhanced Antarctic ozone depletion [*Solomon et al*., 2016].

The free-running FR-WACCM simulations extend from 1955 through 2099 and included an interactive ocean. One set of runs includes time-varying greenhouse gases (GHG) and ozone depleting substances (ODS), while another keeps GHG fixed at 1960 conditions but includes time-varying ODS concentrations (referred to as "ODS only"). A third set keeps ODS fixed at 1960 conditions but includes time-varying GHG (referred to as "GHG only"). Each set has an ensemble of three simulations commencing from slightly differing initial air temperatures (using the approach described in *Kay et al*. [2015]). *Calvo et al*. [2017] show that the CCMI version of WACCM4 used here provides a good simulation of the seasonal cycle of temperature trends in the depletion era, including the maximum cooling in November in peak depletion region near 70 hPa and the warming above the cooling observed near 10–30 hPa (see below). This indicates that the seasonal dynamical and thermal responses to ozone forcing that are the focus of this paper are broadly captured by the model we used. *Calvo et al*. [2017] and *Garcia et al*. [2017] discuss in detail the sensitivity of these results to uncertainties in orographic gravity wave parameterizations.

We also employ output from two long preindustrial control runs of FR-WACCM with CAM5 physics [*Mills et al*., 2016], coupled to Parallel Ocean Program version 2 [*Danabasoglu et al*., 2012] and the Los Alamos National Laboratory sea ice model version 4 [*Holland et al*., 2012]. The control runs are used to estimate the influences of internal and solar natural variability on ozone trends of lengths L1 and L2. This allowed us to generate sampling distributions of ozone trends arising from natural variability. These distributions rely on nonoverlapping segments of the control run time series. Volcanoes were not included in either control run. Results are analyzed for 1000 years of a preindustrial control run that included natural forcing from the 11 year solar cycle (NAT) and for 200 years of a preindustrial control with no temporal changes in solar forcing, which provides an estimate of internal climate variability (CTL). We use these simulations to estimate the likelihood that natural causes alone could explain the trends obtained in Antarctic ozone in the pre-2000 and post-2000 eras in the FR-WACCM simulations. Table 1 presents a summary of all of the model runs considered in this paper and the nomenclature used to identify them.

3. Results and Discussion

Figure 1 shows the seasonal cycle of observed monthly ozone trends at the 70 and 150 hPa levels at South Pole and Syowa stations during the depletion and healing eras. The seasonal and vertical structures of the lower stratospheric ozone trends in the two eras display strikingly similar but mirrored patterns (i.e., reverse sign but similar structure, albeit with some differences in detail). Summer season ozone mixing ratio trends (December-January-February) are of the order of −10 to −30% per decade in the depletion era compared to +5 to +15% per decade in the healing era. In January and February, larger depletion is found at the higher pressure (lower altitude), suggesting that the mean circulation transports the ozone losses downward with time. The maximum depletion era trends of about −20 to −40% per decade occur in September-October at 70 hPa, but at the higher pressure of 150 hPa, the maximum is delayed to November and December. The maximum healing era trends are about +10 to +35% per decade at 70 hPa in the same months and

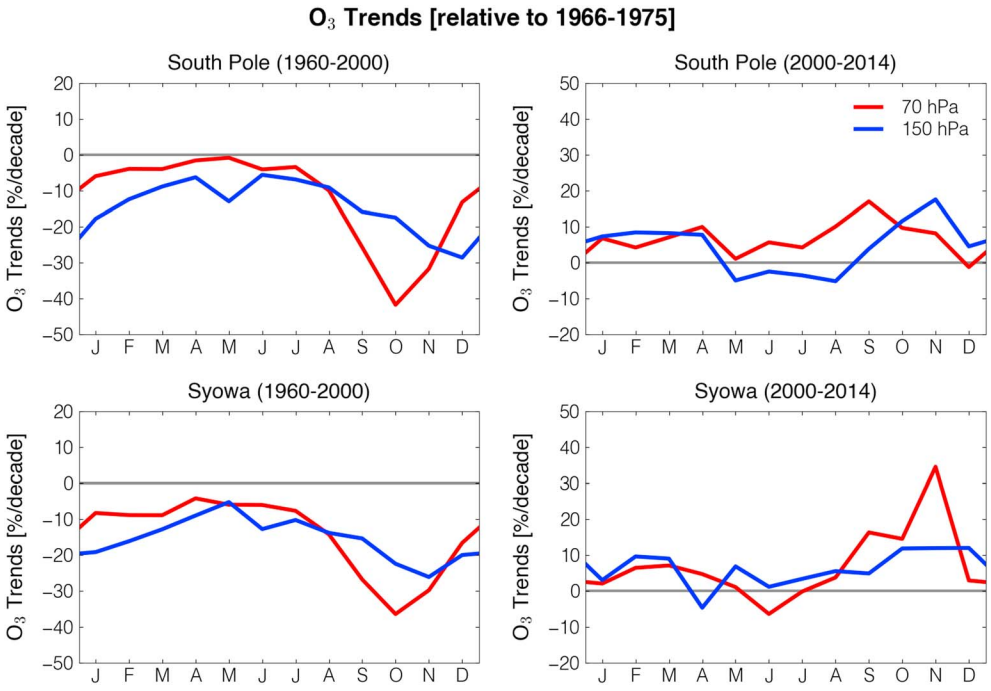

Figure 1. Observed seasonality of ozone trends (% per decade by month) at different pressures in the lower stratosphere from South Pole and Syowa stations. Results are shown over the (left) depletion era (1960–2000) and (right) healing era (2000–2014, excluding 2002), normalized to a 1966–1975 base period (see text).

show similar delays and changes in magnitude at 150 hPa. While there are particular months that represent exceptions at one station or the other, the broad features of the trends in the two eras are largely symmetric with altitude and season, suggestive of common processes acting in reverse. These features are not strongly dependent upon the choice of specific start and end dates for the trends in the two eras (see Figure S1 in the supporting information).

Figure 2 presents corresponding ensemble-mean modeled trends in ozone from the FR-WACCM and SD-WACCM simulations; these were also normalized to a reference period of 1966–1975, with the SD-WACCM simulation being normalized to the CCMI baseline. Both the free-running and specified dynamic WACCM simulations display qualitatively similar patterns to the observations. The key features of these patterns are seasonal reversals of trends between the two eras as well as time lags between the maximum values at 70 and 150 hPa (which are thought to reflect the time required for the most depleted air near 70 hPa to descend via the mean meridional circulation).

An important result of Figure 2 is the general agreement between the ensemble-mean coupled model results (top) and the simulations constrained to the reanalysis temperature and winds (bottom). This comparison supports the view that the general trends of depletion (negative trends) until 2000 and healing (positive trends) after 2000 have substantial contributions from forced responses to changes in anthropogenic ozone depleting substances, although smaller contributions from internal variability and natural solar forcing cannot be ruled out (but see below for analysis of this possibility using the long control runs).

Figure 3 shows the simulated monthly ozone trends at the model levels nearest to 70 and 150 hPa, spatially averaged over 75°S to 90°S. Results are from five different sets of FR-WACCM simulations with and without anthropogenic forcings. A key feature of these results is that in both eras, the ozone trends in the GHG only and unforced simulations are markedly smaller than in the observations. The ODS only and ODS + GHG runs yield ozone trends that are substantially larger and are in general accord with the observations in Figure 1. These results suggest that ODS forcing is the predominant driver of the mirrored changes.

Figures 3 and S2 also provide information on the relative sizes of the human and natural contributions to the mirrored trends in ozone. The natural contributions are estimated from the long CTL and NAT simulations. In each of these simulations, ozone trends were calculated from consecutive nonoverlapping 22 and 15 year

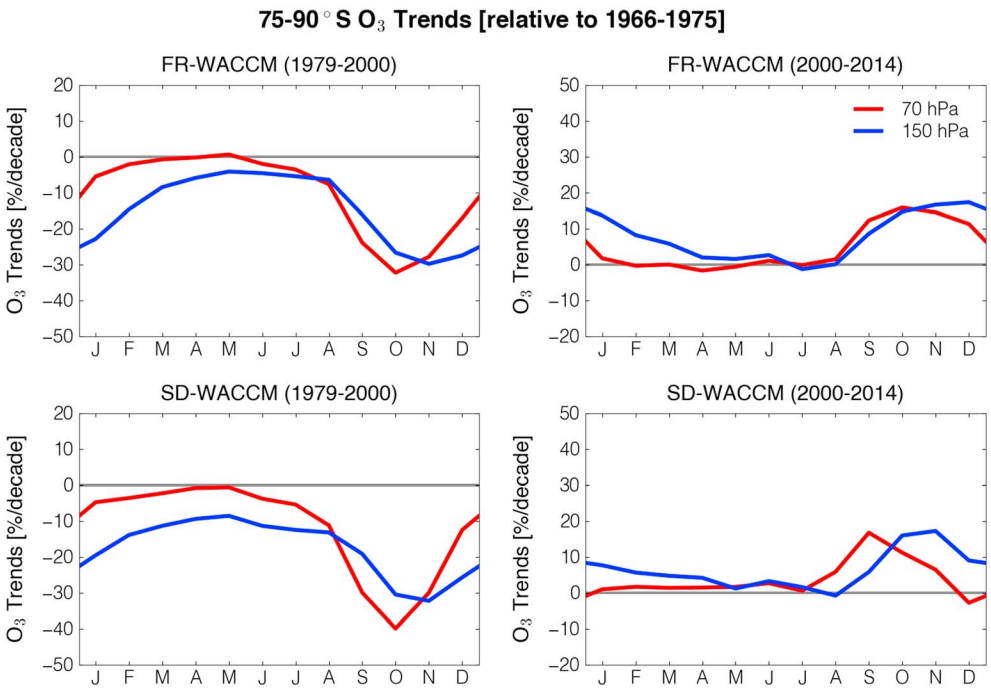

Figure 2. Modeled polar-cap average (75-90S) seasonality of ozone trends (% per decade by month) at different pressures in the lower stratosphere, from the (top) ensemble mean free-running (FR) simulations and the (bottom) specified-dynamics SD-WACCM simulations. Results are shown for the (left) depletion era (1979–2000) and (right) healing era (2000–2014, excluding 2002), normalized to a 1966–1975 base period simulation (see text).

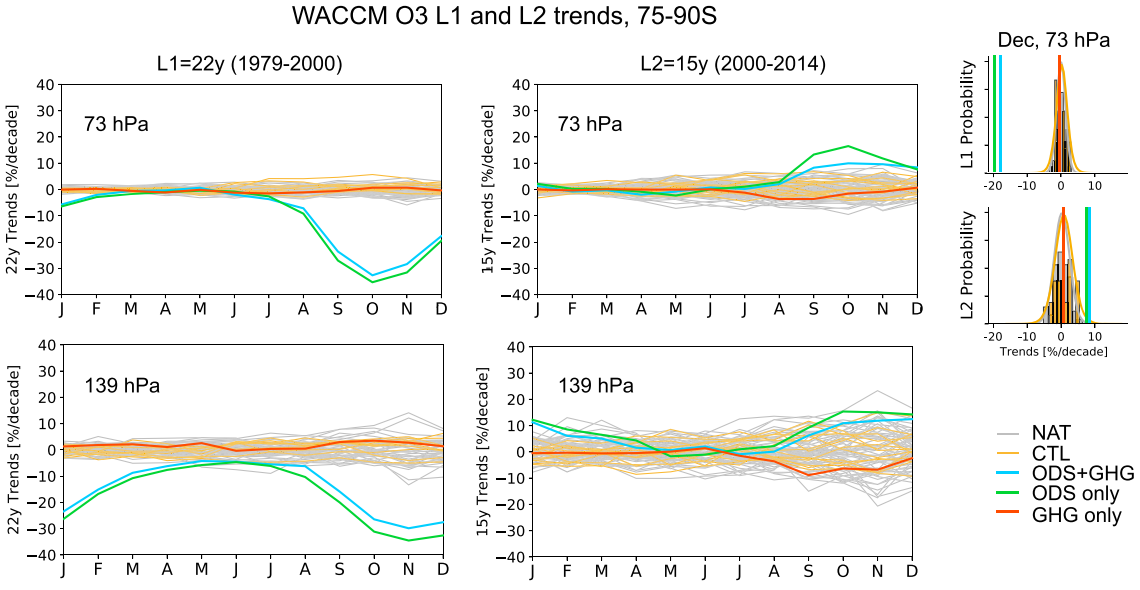

Figure 3. Modeled polar-cap average (75-90S) seasonality of ozone trends (% per decade by month) at 73 and 139 hPa in the lower stratosphere for 22 year (L1) and 15 year (L2) segments. The solid heavy colored lines show the ensemble means of forced FR-WACCM simulations for the depletion era and healing eras (denoted L1 and L2, respectively) including both ODS and GHG forcing (cyan), ODS only (green), and GHG only (red). The light lines show consecutive nonoverlapping L1- and L2-length segments in the long control runs for solar plus internal variability (NAT, light gray) and internal variability only (CTL, light orange). The probability distributions of the long control run trends for the month of December at 73 hPa only are shown in the small histograms at the right, together with the December trends from the ODS + GHG, ODS only, and GHG only simulations. The smooth curves in the histogram figure show the NAT and CTL distributions modeled with a Student's *t* distribution (based on the distribution of individual segments).

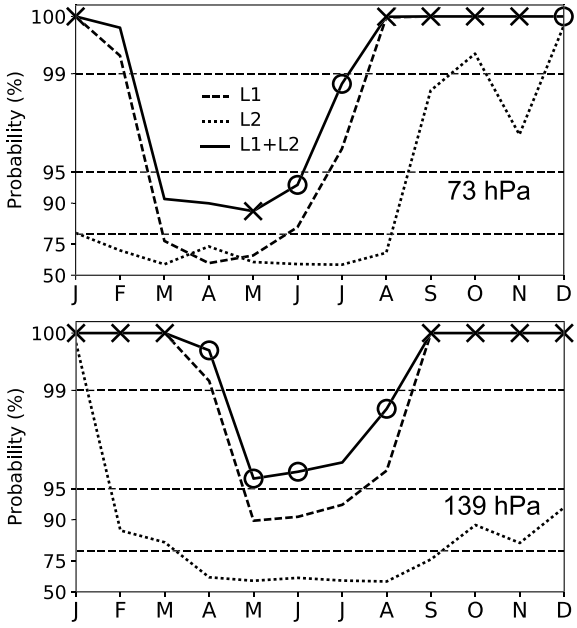

Figure 4. Probabilities of the monthly FR-WACCM ODS + GHG ozone trends at two pressure levels not being found in model runs including only natural and internal climate variability (see text) shown as the dashed line for the depletion era (L1), while the probability for the healing era is shown by the dotted line (L2). The probability of obtaining the L1 trends followed consecutively by the L2 trends is also shown by the solid line, with "X" marking the months where the sign of the trend switched from L1 to L2 in both the model and at the two stations shown in Figure 1. "O" marks months where this occurred in the model only. The absence of "X" or "O" markings indicates that there was no change in the sign of the trend between L1 and L2 in FR-WACCM ODS + GHG.

segments (corresponding to the L1 and L2 periods, respectively). The NAT simulation contained 44 and 66 nonoverlapping trends for the L1 and L2 periods (respectively), while the CTL had sample sizes of 9 and 13 trends. These data were used to construct probability density functions (PDFs), using a Student's *t* distribution based on the standard deviation and mean of the sampled trends for L1 and L2. While trends in the ODS and ODS + GHG simulations are larger in September and October compared to other months, so is the variability (as shown by the CTL and NAT simulations). Particularly in the L2 period, the forced trends are therefore best distinguished from variability in the more quiescent month of December.

The probability distributions of the ozone trends from the CTL and NAT simulations are illustrated in the small histograms at the right-hand side of Figure 3 for 73 hPa. Because of the above-described favorable signal-to-noise properties in December, the PDFs shown in Figure 3 are for this specific month; PDFs for additional months (and for 139 hPa) are presented in Figure S2. These distributions can be compared with the vertical colored lines, which denote the ensemble mean trends from the ODS only, GHG only, and ODS + GHG simulations. This comparison suggests that in the WACCM model, calculated ozone trends during much of austral spring and summer are unlikely to be explained by either internal variability alone or by the combined effects of internal variability and solar forcing (see below for further quantification). This result holds for both the post- and the pre-2000 periods and for both pressure levels.

Our subsequent analysis of the statistical significance of changes in ozone trends between the depletion and recovery periods assesses the probability that this "mirroring" behavior could be due to natural causes alone. We rely on the NAT and CTL runs to estimate this probability. As a prelude to this analysis, it is necessary to determine whether we can consider sequential L1- and L2-length ozone trends to be statistically independent (see Figure S3), or whether any significant dependence could be introduced by multidecadal internal variability and solar forcing. We find that sequential L1 and L2 length trends are virtually uncorrelated (with, for example, correlation coefficients for November through February for 73 hPa ranging from −0.086 to 0.084 and for 139 hPa from −0.098 to 0.079).

Figure 4 expands on these findings and examines whether the sequential L1 and L2 ozone trends obtained using the three member ODS + GHG ensemble for the depletion and healing eras could occur through the combined effects of internal and natural solar variability. The analysis relies on the above-described sampling distributions of the CTL and NAT ozone trends for analysis time scales of lengths L1 and L2. As in Figure 3, the Student's *t* probability density functions of the control runs are constructed for each month, but with both NAT and CTL sampled trends combined to increase sampling sizes. To estimate the probabilities shown in Figure 4, we integrate these PDFs over ranges greater than or equal to the magnitude (preserving the sign) of the calculated ODS + GHG trends. Probabilities are estimated separately for ODS + GHG trends of lengths L1 in the depletion era and of length L2 in the healing era.

The probabilities displayed in Figure 4 show the likelihood of the ODS + GHG trends not being found in NAT and CTL, estimated separately for both the L1 and L2 length trends. Additionally, the likelihood of obtaining the L1 ozone trend followed by the L2 trend was calculated by multiplying the individual L1 and L2 likelihoods; this is akin to the probability of getting heads or tails in sequential and uncorrelated coin tosses (as noted above, there is virtually no correlation between sequential L1 and L2 ozone trends in either NAT or CTL). The sign change between L1 and L2 is shown in Figure 4 (as the solid "L1 + L2" line) for each individual month. These results support the view that the ozone changes in the depletion and healing eras are not random but instead reflect a common forced response that differs from preindustrial times (i.e., mirroring as defined in this paper).

Whenever a sign reversal between L1 and L2 is present (mirroring) in both the observations (as measured at both stations in Figure 1) and the ensemble mean ODS + GHG trends, it is indicated by an "X," while "O" denotes months when a sign reversal occurs in the model ODS + GHG simulation only. Chemical ozone depletion is well known to be largest in the austral spring months of September, October, and November, with residual depletion lasting through the summer (December, January, and February) and much less change in austral fall and winter (see, e.g., *Solomon*'s [1999] review, and references therein). If mirroring occurs through forced responses to ODS decreases, it should follow the same basic seasonal pattern. The L1 + L2 results in Figure 4 are consistent with these expectations.

Consider the L1 results first. At 73 hPa, 8 of the 12 monthly trends in the ODS + GHG simulation are statistically significant at the 95% level or better. In each of these 8 months, therefore, there is less than a 1 in 20 chance that the combined effects of internal variability and solar irradiance changes could explain the WACCM-simulated ODS + GHG ozone decreases in the L1 period. Even smaller probabilities are obtained in August through February. In these months, it is a virtual certainty that the modeled trend cannot be explained by internal or solar variability and hence must be forced by other processes. Only 4 months (March through June, inclusive) display decreases in ozone in the depletion era that fail to achieve statistical significance at the 95% level or better. This is consistent with expectations from the seasonal character of the ozone hole chemistry. At 139 hPa, 9 out of 12 months have statistically significant ozone decreases at the 95% level or better in the depletion era; the only nonsignificant ozone trends occur in May, June, and July.

The positive trends in ozone during the shorter L2 healing era (in the ODS + GHG simulation) yield fewer statistically significant results than in the L1 period. Nonetheless, at 73 hPa, 4 out of 12 months display ozone increases that are statistically significant at the 95% level or better. In particular, these occur in the key (and consecutive) months of September, October, November, and December, providing confidence that these healing trends are also forced by changes in ODS. One common feature of the L1 and L2 results is that the higher altitude level displays more monthly trends that are statistically unusual relative to the CTL and NAT trends, consistent with the reduced variability seen in that level in Figure 3.

Figure 4 also indicates that considering changes in the sign of the ozone trends between the L1 and L2 periods makes it even more difficult to explain the observed trends by natural causes. At both the 73 and 139 hPa levels, all of the months lying between August and January show changes in the sign of the ozone trend. Internal variability alone would be expected to produce random changes in the sign of ozone trends between the L1 and L2 periods but is unlikely to replicate the ODS + GHG (and the observed) pattern of negative ozone trends in L1 followed by positive ozone trends in L2 at the magnitudes shown. Although solar forcing on 11 year time scales (in the NAT simulation) could, in principle, generate nonrandom decadal changes in the sign of the ozone trends, the evidence from Figure 4 is that the combined effects of solar forcing and internal variability are inconsistent with the observed mirroring behavior.

Figure 5 shows the temperature trends in the depletion and healing eras in the MERRA reanalysis and in the ensemble means of the free-running WACCM simulations with ODS + GHG forcings. Trends obtained in the lower stratosphere in the ODS only case are similar. Between 200 and 50 hPa, both WACCM and the reanalysis data shown in Figure 5 have broadly similar seasonal patterns of temperature trends apart from strong warming seen in the observations in February–April above about 100 hPa. Both also show pronounced "mirroring" of temperature trends in the L1 and L2 periods, including a mirrored tongue of continuing cooling (or warming) near 100–200 hPa at least through February. While there are differences in detail between the model and the observations (discussed further below), the temperature change patterns provide complementary evidence that a forced process is acting in reverse before and after 2000 in the lower stratosphere where

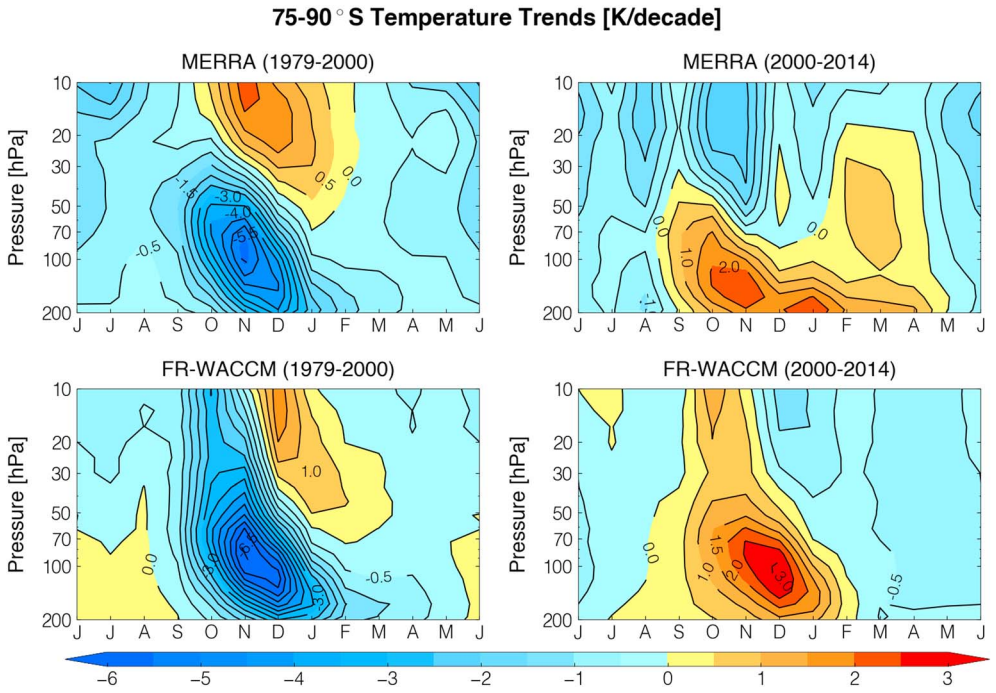

Figure 5. Observed seasonal trends in temperature (K per decade) averaged over 75-90S from MERRA and the ensemble mean FR-WACCM model simulations, for the (left) depletion era (1979–2000) and the (right) healing era (2000–2014, excluding 2002).

ODS-forced changes are largest. Larger differences are seen at higher altitudes, although it should be noted that uncertainties in MERRA temperatures may increase at levels above 30 hPa or so because of fewer radiosondes reaching these levels to provide assimilation data, particularly in Antarctic winter. The higher altitudes are discussed further below.

Previous work has shown that a useful signature of dynamical change is warming above the maximum in ozone-induced cooling in the depletion era [*Calvo et al.*, 2012, 2017]. Beginning around December, warming is manifest near 30–50 hPa, signaling enhanced downwelling in both WACCM and MERRA in the depletion era (Figure 5). This appears to be mirrored in a cooling above the warming during the healing era, a feature of both the observations and the ensemble mean of the free-running model between December and January. The stronger higher level cooling in MERRA in October and November during the healing era suggests reduced downwelling at these levels that does not occur in the ensemble-mean FR-WACCM simulations. Another difference in the healing era results is the coherent warming (from about 20 to 200 hPa) observed in MERRA from February to May, which is also absent in the FR-WACCM simulations. Both of these discrepancies between observed and free-running modeled temperature trends support a significant role for dynamical variability, addressed further below.

The spectroscopy of ozone is well-established, and radiative calculations can be used to estimate the temperature changes driven by ozone changes. *Ivy et al.* [2016] applied the seasonally evolving fixed dynamical heating approach of *Forster and Shine* [1997] to derive radiatively driven temperature trends in the ozone depletion era using the radiative submodel of WACCM (PORT). We take the same approach here to evaluate how much of the warming in the healing era can be attributed to the radiative effects of ozone changes. To do this, we apply the ozone changes in SD-WACCM chemistry simulations discussed in *Solomon et al.* [2016] to PORT. GHG changes over the period are not included in these calculations; ozone is the sole driver of radiative effects that are considered here. *Ivy et al.* [2016] showed that GHG-induced cooling using PORT were smaller than 0.5 K/decade and had little seasonal structure; these changes are relatively small compared to the features of interest (see below). The SD-WACCM simulations provide two estimates of ozone changes post-2000: using time-evolving chemistry plus dynamics/temperature driven by MERRA reanalysis data (chem-dyn-vol) and using time-evolving chemistry alone (chem-only). In the latter case, we hold dynamics

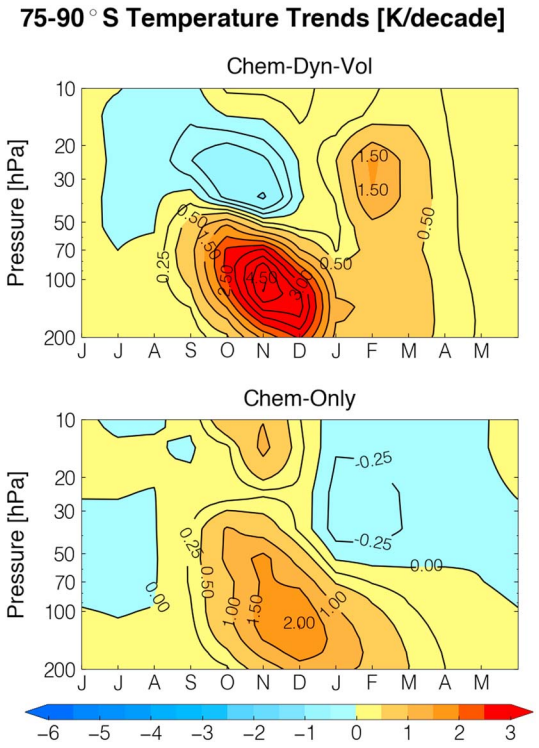

Figure 6. Calculated temperature trends (K per decade) due only to the radiative impact of calculated ozone trends obtained in SD-WACCM nudged to MERRA from 2000 to 2014 using the PORT radiative transfer code. (top) Calculations for the case including chemistry, dynamics/temperature, and volcanism (chem-dyn-vol) and (bottom) those due only to chemistry changes alone over 2000–2014 (chem-only).

and temperature fixed at year 1999 values and allow ozone to be driven solely by chemistry, i.e., by the decline of ozone-depleting substances (see *Solomon et al.* [2016] for details). We exclude the year 2015 in order to avoid significant impacts from the Calbuco volcano; apart from this year, volcanic effects on ozone as shown in *Solomon et al.* [2016] are small.

These two calculations are designed to reveal how much temperature change in the healing era is radiatively driven by ozone changes linked solely to chemistry, as compared to the ozone changes obtained from chemistry along with MERRA reanalysis dynamics/temperature. Figure 6 shows these radiative components of the seasonal and vertical structure of temperature trends, spatially averaged over the polar cap. According to Figure 6, radiative response and feedbacks to the ozone trends can be expected to make important contributions to the warming trends in southern high latitudes in the healing era. It should be emphasized that temperature and ozone changes are linked by temperature-dependent chemistry, such that a 1 K temperature change can yield 10–15% increases in ozone in the lowermost stratosphere, particularly in October [see *Solomon et al.*, 2015, Figure 6]. Thus, the radiative temperature trends indicated in the chem-only panel in Figure 6 imply that temperature feedbacks driven by the ozone changes have made some contribution to the healing of the Antarctic ozone hole.

Comparison of the two panels in Figure 6 shows how differences in calculated ozone driven by changes in dynamics and temperature in the MERRA reanalysis post-2000 feedback to temperature. Some features in the FR-WACCM results appear to be more similar to the chem-dyn-vol simulation than to the chem-only simulation, attesting to the radiative impact of transported ozone: for example, the warming exceeds 2 K per decade from November to February near 100 hPa in both chem-dyn-vol and FR-WACCM. However, an ozone-induced warming is obtained in February to March from 100 to 30 hPa in the chem-dyn-vol simulation (similar to that in MERRA, Figure 5) but is absent in FR-WACCM, suggesting that it is driven mainly by ozone changes that are themselves linked to dynamics and temperature changes in the MERRA reanalysis. However, there are also many differences between the chem-dyn-vol results in Figure 6 and the MERRA data shown in Figure 5, such as the strong cooling obtained at 50–30 hPa in November. Assuming that the calculated ozone distribution in the chem-dyn-vol simulation is accurate, these differences strongly suggest that dynamical processes make important contributions to the observed thermal changes in the recovery era, for example, in November when the strong cooling in the MERRA data suggests a dominant effect of reduced downwelling. Reduced downwelling would, in turn, be expected to reduce ozone, making a secondary contribution to cooling through ozone radiative processes (consistent with the cooling in November near 40 hPa seen in the top panel of Figure 6). It remains possible, however, that some dynamical changes could be driven by the ozone changes (e.g., changes to the overturning circulation driven by ozone changes or ozone chemistry changes linked to dynamics and temperature changes in the reanalysis that also feedback to the temperature effects). Further analysis of these possibilities is outside the scope of the present work.

4. Conclusions

Observed ozone and temperature trends in the Antarctic lower stratosphere (at 70 and 150 hPa) during the depletion and healing eras display striking symmetry, with reductions in ozone and decreases in temperatures in the 20th century transitioning to increased ozone and warming in the 21st. The "mirror image" structures of these altitudinal/seasonal patterns point toward common processes of opposite sign acting in the two eras. When forced by historical changes in ODS and GHGs, the WACCM4 coupled chemistry-climate model displays similar mirror image behavior in the depletion and healing eras, both for the calculated changes in Antarctic ozone and temperature. These results provide compelling evidence that the bulk of the mirrored changes are forced responses to the increases and decreases in ozone depleting substances over time.

Long preindustrial control runs of WACCM were used to determine whether ozone trends in the 22 year depletion era and 15 year healing era are statistically unusual relative to ozone trends arising from solar and internal variability. We also considered whether changes in the sign of ozone trends in the two eras could be plausibly explained by natural causes. All of these tests support the conclusion that the mirroring of trends in the two eras is very likely to be forced. Further, model runs with forcing by ODS only, GHG only, and ODS + GHG support the dominant role of ODS forcing.

As ozone changes, temperature feedbacks are expected to occur, and the comparisons of observed temperature changes between the two eras to radiative calculations highlight the importance of ozone in the thermal budget. Radiative calculations suggest that a portion of the observed warming trend at high southern latitudes is linked to chemically driven ozone increases as captured in a chemistry-only simulation in the healing era. However, changes both in ozone and in temperature itself linked to dynamics appear to make larger contributions.

In summary, our analysis provides evidence from both temperature and ozone trends that the healing of the Antarctic ozone hole has begun. This recovery is evident in both observations and state-of-the-art model simulations. Our findings illustrate the importance of coupling among chemistry, radiation, and dynamics and show that many of the seasonal and altitudinal patterns of changes in the ozone trends are very unlikely to be occurring by chance. As anthropogenic ODS content continues to decrease in the Earth's atmosphere, and as the healing era lengthens, the mirrored patterns presented here can be expected to become even clearer. The approach taken in this paper therefore presents a framework for future analysis to document the efficacy of the Montreal Protocol over time.

Acknowledgments

D.E.K. and S.S. were partially supported by NSF FESD grant OCE-1338814, and D.I. was partially supported by NSF Atmospheric Chemistry Division grant 1539972. J.B. acknowledges support by NSF Climate and Large-Scale Dynamics Division grant 1419667. The National Center for Atmospheric Research (NCAR) is sponsored by the U.S. National Science Foundation. WACCM is a component of the Community Earth System Model (CESM), which is supported by the National Science Foundation (NSF) and the Office of Science of the U.S. Department of Energy. Computing resources were provided by NCAR's Climate Simulation Laboratory, sponsored by NSF and other agencies. This research was enabled by the computational and storage resources of NCAR's Computational and Information System Laboratory (CISL). We thank NASA Goddard Space Flight Center for the MERRA data (accessed freely online at http://disc.sci.gsfc.nasa.gov/). We also thank the South Pole and Syowa ozone teams for the data used in this paper, available at NOAA; esrl.noaa.gov/gmd/dv/spo_oz) and World Ozone and Ultraviolet Radiation Data Centre (WOUDC; woudc.org) archives, respectively. Model results shown in this paper are available on request to the WACCM liason, Michael Mills (mmills@ucar.edu).

References

Arfeuille, F., B. P. Luo, P. Heckendorn, D. K. Weisenstein, J. X. Sheng, E. Rozanov, M. Schraner, S. Brönnimann, L. W. Thomason, and T. Peter (2013), Modeling the stratospheric warming following the Mt. Pinatubo eruption: Uncertainties in aerosol extinctions, *Atmos. Chem. Phys.*, *13*(22), 11,221–11,234, doi:10.5194/acp-13-11221-2013.

Butchart, N., et al. (2010), Chemistry-climate model simulations of twenty-first century stratospheric climate and circulation changes, *J. Clim.*, *23*, 5349–5374, doi:10.1175/2010JCLI3404.1.

Cai, W. (2006), Antarctic ozone depletion causes an intensification of the Southern Ocean super-gyre circulation, *Geophys. Res. Lett.*, *33*, L03712, doi:10.1029/2005GL024911.

Calvo, N., R. R. Garcia, D. R. Marsh, M. J. Mills, D. E. Kinnison, and P. J. Young (2012), Reconciling modeled and observed temperature trends over Antarctica, *Geophys. Res. Lett.*, *39*, L16803, doi:10.1029/2012GL052526.

Calvo, N., R. R. Garcia, and D. E. Kinnison (2017), Revisiting southern hemisphere polar stratospheric temperature trends in WACCM: The role of dynamical forcing, *Geophys. Res. Lett.*, *44*, 3402–3410, doi:10.1002/2017GL072792.

Conley, A. J., J.-F. Lamarque, F. Vitt, W. D. Collins, and J. Kiehl (2013), PORT, a CESM tool for the diagnosis of radiative forcing, *Geosci. Model Dev.*, *6*, 469–476, doi:10.5194/gmd-6-469-2013.

Danabasoglu, G., S. C. Bates, B. P. Briegleb, S. R. Jayne, M. Jochum, W. G. Large, S. Peacock, and S. G. Yeager (2012), The CCSM4 ocean component, *J. Clim.*, *25*(5), 1361–1389.

Forster, P. M., and K. P. Shine (1997), Radiative forcing and temperature trends from stratospheric ozone changes, *J. Geophys. Res.*, *102*, 10,841–10,855, doi:10.1029/96JD03510.

Garcia, R. R., A. K. Smith, D. E. Kinnison, Á. D. L. Cámara, and D. J. Murphy (2017), Modification of the gravity wave parameterization in the Whole Atmosphere Community Climate Model: Motivation and results, *J. Atmos. Sci.*, *74*(1), 275–291.

Holland, M. M., D. A. Bailey, B. P. Briegleb, B. Light, and E. Hunke (2012), Improved sea ice shortwave radiation physics in CCSM4: The impact of melt ponds and black carbon, *J. Clim.*, *25*(5), 1413–1430, doi:10.1175/JCLI-D-11-00078.1.

Ivy, D., S. Solomon, and H. Rieder (2016), Radiative and dynamical influences on polar stratospheric temperature trends, *J. Clim.*, *29*, 4927–4938, doi:10.1175/JCLI-D-15-0503.1.

Kay, J. E., et al. (2015), The Community Earth System Model (CESM) large ensemble project: A community resource for studying climate change in the presence of internal climate variability, *Bull. Am. Meteorol. Soc.*, *96*, 1333–1349.

Kunz, A., L. L. Pan, P. Konopka, D. E. Kinnison, and S. Tilmes (2011), Chemical and dynamical discontinuity at the extratropical tropopause based on START08 and WACCM analyses, *J. Geophys. Res.*, *116*, D24302, doi:10.1029/2011JD016686.

Lin, P., and Q. Fu (2013), Changes in various branches of the Brewer-Dobson circulation from an ensemble of chemistry climate models, *J. Geophys. Res. Atmos.*, *118*, 73–84, doi:10.1029/2012JD018813.

Lin, P., Q. Fu, S. Solomon, and J. M. Wallace (2009), Temperature trend patterns in southern hemisphere high latitudes: Novel indicators of stratospheric change, *J. Clim.*, *22*, 6325–6341.

Manzini, E., B. Steil, C. Brühl, M. A. Giorgetta, and K. Krüger (2003), A new interactive chemistry-climate model: 2. Sensitivity of the middle atmosphere to ozone depletion and increase in greenhouse gases and implications for recent stratospheric cooling, *J. Geophys. Res.*, *108*(D14), 4429, doi:10.1029/2002JD002977.

Marsh, D. R. (2011), Chemical-dynamical coupling in the mesosphere and lower thermosphere, in *Aeronomy of the Earth's Atmosphere and Ionosphere*, *IAGA Spec. Sopron Book Ser.*, vol. 2, edited by M. Abdu, D. Pancheva, and A. Bhattacharyya, pp. 3–17, Springer, Dordrecht, Netherlands.

Marsh, D. R. M. J., D. E. Mills, J. F. Kinnison, N. C. Lamarque, and L. M. Polvani (2013), Climate change from 1850 to 2005 simulated in CESM1 (WACCM), *J. Clim.*, *26*, 7372–7391, doi:10.1175/JCLI-D-12-00558.1.

McLandress, C., A. I. Jonsson, D. A. Plummer, M. C. Reader, J. F. Scinocca, and T. G. Shepherd (2010), Separating the dynamical effects of climate change and ozone depletion. Part I: Southern Hemisphere stratosphere, *J. Clim.*, *23*, 5002–5020, doi:10.1175/2010JCLI3586.1.

Mills, M. J., et al. (2016), Global volcanic aerosol properties derived from emissions, 1990–2014, using WACCM5, *J. Geophys. Res. Atmos.*, *121*, 2332–2348, doi:10.1002/2015jd024290.

Morgenstern, O., et al. (2017), Review of the global models used within phase-1 of the Chemistry-Climate Model Initiative (CCMI), *Geosci. Model Dev.*, *10*, 639–671, doi:10.5194/gmd-10-639-2017.

Oberländer-Hayn, S., S. Meul, U. Langematz, J. Abalichin, and F. Haenel (2015), A chemistry-climate model study of past changes in the Brewer-Dobson circulation, *J. Geophys. Res. Atmos.*, *120*, 6742–6757, doi:10.1002/2014JD022843.

Ramaswamy, V., M. D. Schwarzkopf, and W. J. Randel (1996), Fingerprinlt of ozone depletion in the spatial and temporal pattern of recent lower stratospheric cooling, *Nature*, *382*, 616–618.

Randel, W. J., and F. Wu (1999), Cooling of the Arctic and Antarctic polar stratospheres due to ozone depletion, *J. Clim.*, *12*, 1467–1479.

Rienecker, M. M., et al. (2011), MERRA: NASA's Modern-Era Retrospective Analysis for research and applications, *J. Clim.*, *24*, 362–3648, doi:10.1175/JCLI-D-11-00015.1.

Rex, M., R. J. Salawitch, P. von der Gathen, N. R. P. Harris, M. P. Chipperfield, and B. Naujokat (2004), Arctic ozone loss and climate change, *Geophys. Res. Lett.*, *31*, L04116, doi:10.1029/2003GL018844.

Scaife, A. A., D. R. Jackson, R. Swinbank, N. Butchart, H. E. Thornton, M. Keil, and L. Henderson (2005), Stratospheric vacillations and the major warming over Antarctica in 2002, *J. Atmos. Sci.*, *62*, 629–639.

Shine, K. (1986), On the modelled thermal response of the Antarctic stratosphere to a depletion of ozone, *Geophys. Res. Lett.*, *13*, 1331–1334.

Sinnhuber, B. M., G. Stiller, R. Ruhnke, T. von Clarmann, S. Kellmann, and J. Aschmann (2011), Arctic winter 2010/2011 at the brink of an ozone hole, *Geophys. Res. Lett.*, *38*, L24814, doi:10.1029/2011GL049784.

Solomon, S. (1999), Stratospheric ozone depletion: A review of concepts and history, *Rev. Geophys.*, *37*, 275–316, doi:10.1029/1999RG900008.

Solomon, S., R. W. Portmann, T. Sasaki, D. J. Hofmann, and D. W. J. Thompson (2005), Four decades of ozonesonde measurements over Antarctica, *J. Geophys. Res.*, *110*, D21311, doi:10.1029/2005JD005917.

Solomon, S., D. Kinnison, J. Bandoro, and R. Garcia (2015), Simulation of polar ozone depletion: An update, *J. Geophys. Res. Atmos.*, *120*, 7958–7974, doi:10.1002/2015JD023365.

Solomon, S., D. J. Ivy, D. Kinnison, M. J. Mills, R. R. Neely III, and A. Schmidt (2016), Emergence of healing in the Antarctic ozone layer, *Science*, *353*, 269–274.

Son, S.-W., N. F. Tandon, L. M. Polvani, and D. W. Waugh (2009), Ozone hole and southern hemisphere climate change, *Geophys. Res. Lett.*, *36*, L15705, doi:10.1029/2009GL038671.

Thompson, D. W. J., and S. Solomon (2002), Interpretation of recent southern hemisphere climate change, *Science*, *296*, 895–899, doi:10.1126/science.1069270.

Journal of Geophysical Research

Supporting Information for

Mirrored Changes in Antarctic Ozone And Temperature in the 20th versus 21st Centuries

Susan Solomon[1], Diane Ivy[1], Mukund Gupta[1], Justin Bandoro[1], Benjamin Santer[2], Qiang Fu[3], Pu Lin[4], Rolando R. Garcia[5], Doug Kinnison[5], Michael Mills[5]

[1]Department of Earth, Atmospheric, and Planetary Sciences, Massachusetts Institute of Technology, Cambridge, MA 02139

[2]Program for Climate Model Diagnosis and Intercomparison (PCMDI), Lawrence Livermore National Laboratory, Livermore, CA 94550

[4]Dept. of Atmospheric Sciences, University of Washington, Seattle, WA 98195

[5]NOAA Geophysical Fluid Dynamics Laboratory, Princeton Forrestal Campus, Princeton, NJ 08540

[5]Atmospheric Chemistry Observations and Modeling Laboratory, National Center for Atmospheric Research, Boulder, CO 80307

Contents of this file

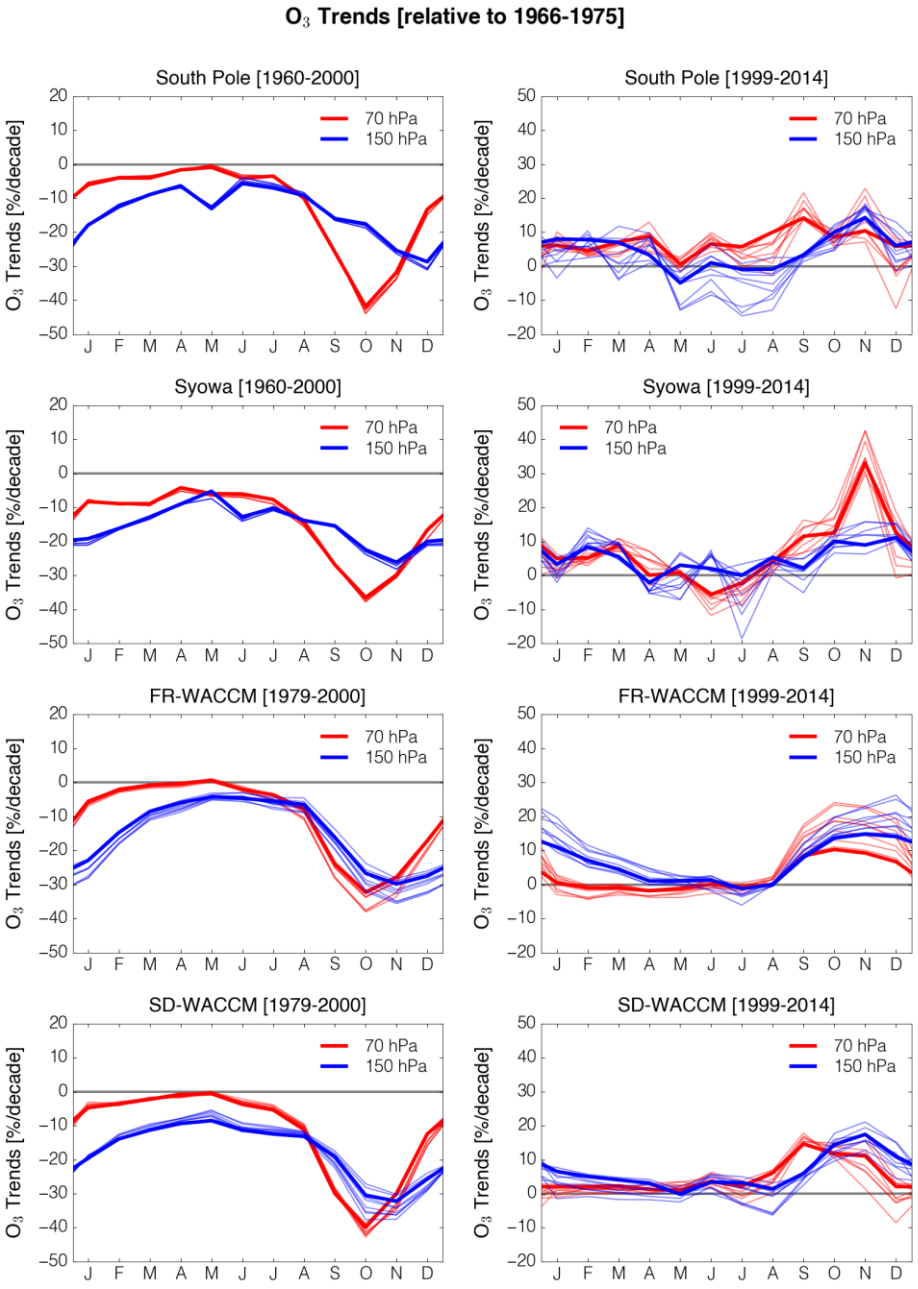

Figure S1. Tests of the sensitivity of ozone trends at 70 and 150 hPa to changes in the start and end years. In each case, the trend start year has been increased or decreased by one year, and the corresponding end year has been both increased and decreased by one year, to test sensitivities to the length of the trend periods and the specific choices of years. Results are shown over the depletion era on the left (for example, at South Pole and Syowa for start dates of 1961±1 year coupled with end dates of 1999±1 year) and healing era on the right (with start dates of 1999±1 year coupled with end dates of 2013±1 year). All results are normalized to a 1966-1975 base period.

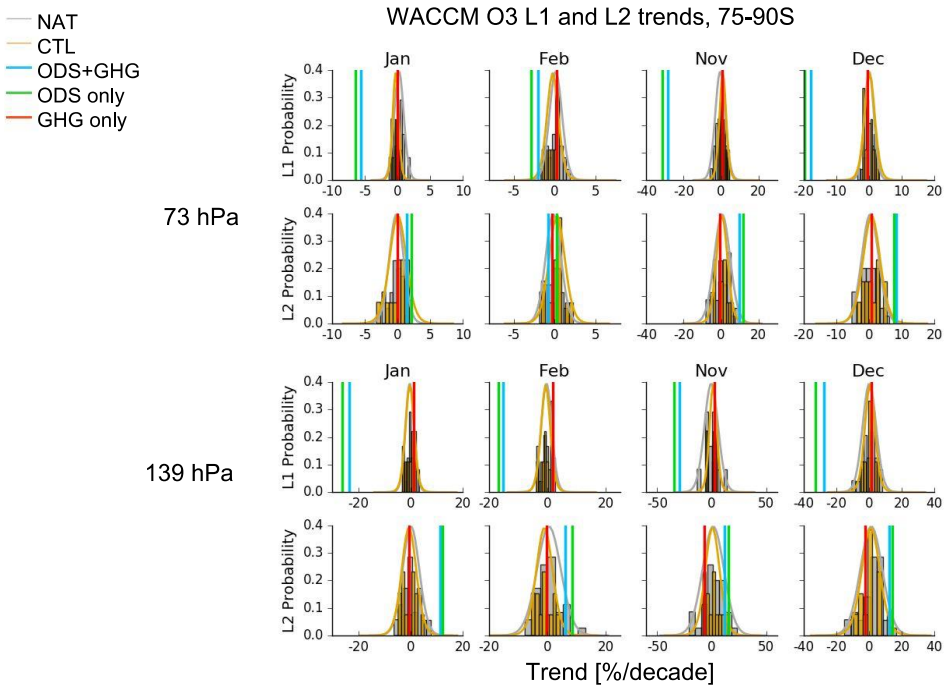

Figure S2. Probability density functions for L1- and L2-length ozone trends calculated from the long control run. Results are for selected months of the year and for two different pressure levels (73 and 139 hPa). For each month and pressure level, depletion era trends are on top and the healing era trends are shown below. The smooth curves are fits to the NAT and CTL trend sampling distributions assuming an underlying Student's-t distribution. Vertical lines are the L1- and L2-era trends inferred from the ODS+GHG, ODS only, and GHG only simulations (see Fig. 3).

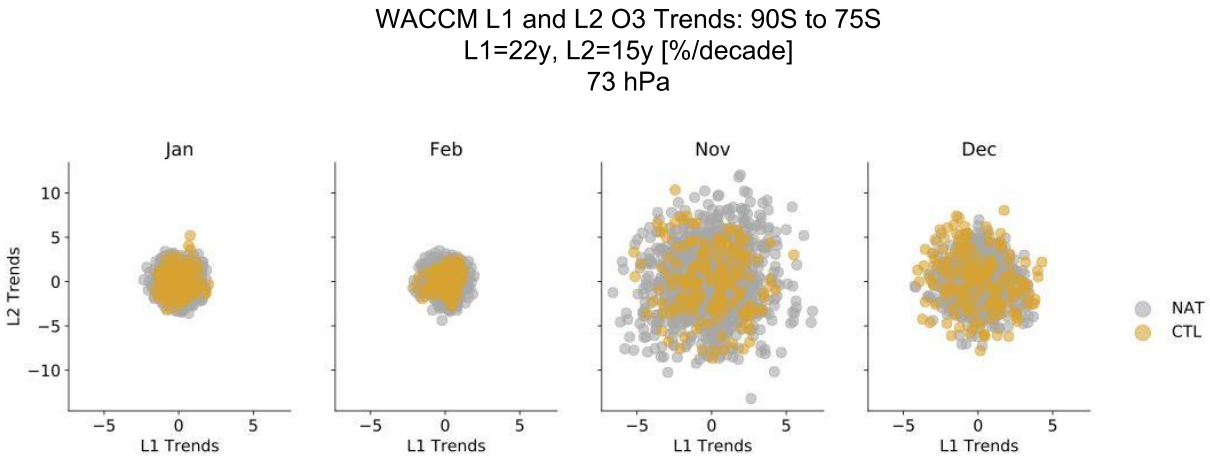

Figure S3. Scatterplot of sequential L1- and L2-length ozone trends in the austral summer and fall from the NAT and CTL runs. Results are in percent per decade, and are for the 139 hPa level. The figure shows that in these two simulations, sequential L1- and L2-length trends are virtually uncorrelated.